Data-driven approaches improve Tau-PET biomarkers in Alzheimer's disease

Jacob W. Vogel, BA[1,2]*, Niklas Mattsson, MD, PhD[3,4,5], Yasser Iturria-Medina, PhD[1], T. Olof Strandberg, PhD[3], Michael Schöll, PhD[3,6], Christian Dansereau, PhD[7,8], Sylvia Villeneuve, PhD[1,9], Wiesje M. van der Flier, MA[2,10], Philip Scheltens, MD[2], Pierre Bellec, PhD[7,8], Alan C. Evans, PhD[1], Oskar Hansson, MD, PhD[3,4]#, Rik Ossenkoppele, PhD[2,3]#, the Alzheimer's Disease Neuroimaging Initiative** & the Swedish BioFINDER study

[1] Montreal Neurological Institute, McGill University, Montreal, QC, Canada
[2] Alzheimer Center and Department of Neurology, VU University medical center, Amsterdam Neuroscience, Amsterdam, Netherlands
[3] Clinical Memory Research Unit, Lund University, Lund, Sweden
[4] Memory Clinic, Skåne University Hospital, Lund, Sweden
[5] Department of Neurology, Skåne University Hospital, Lund, Sweden
[6] Wallenberg Centre for Molecular and Translational Medicine, University of Gothenburg, Gothenburg, Sweden
[7] Department of Computer Science and Operations research, Université de Montréal, Montreal, QC, Canada
[8] Centre de Recherche de l'Institut Universitaire de Gériatrie de Montréal, University of Montreal, Montreal, QC, Canada
[9] Department of Psychiatry, McGill University, Montreal, QC, Canada
[10] Department of Epidemiology and Biostatistics, VU University medical center, Amsterdam, Netherlands

# Both authors contributed equally to this work.

* Corresponding author
Jacob W. Vogel
jacob.vogel@mail.mcgill.ca
McGill Centre for Integrative Neuroscience
Montreal Neurological Institute, Room NW145
3801 Boulevard Robert-Bourassa
Montreal, QC H3A 2B4
Canada

** Data used in preparation of this article were obtained from the Alzheimer's Disease Neuroimaging Initiative (ADNI) database (adni.loni.usc.edu). As such, the investigators within the ADNI contributed to the design and implementation of ADNI and/or provided data but did not participate in analysis or writing of this report. A complete listing of ADNI investigators can be found at: http://adni.loni.usc.edu/wp-content/uploads/how_to_apply/ADNI_Acknowledgement_List.pdf

ABSTRACT

Objective: Previous positron emission tomography (PET) studies have quantified filamentous tau pathology using regions-of-interest (ROIs) based on observations of the topographical distribution of neurofibrillary tangles in post-mortem tissue. However, such approaches may not take full advantage of information contained in neuroimaging data. The present study employs an unsupervised data-driven method to identify spatial patterns of tau-PET distribution, and to compare these patterns to previously published "pathology-driven" ROIs. **Method:** Tau-PET patterns were identified from a discovery sample comprised of 123 normal controls and patients with mild cognitive impairment or Alzheimer's disease (AD) dementia from the Swedish BioFINDER cohort, who underwent [^{18}F]AV1451 PET scanning. Associations with cognition were tested in a separate sample of 90 individuals from ADNI. BioFINDER [^{18}F]AV1451 images were entered into a voxelwise clustering algorithm, which resulted in five clusters. Mean [^{18}F]AV1451 uptake in the data-driven, clusters and 35 previously published pathology-driven ROIs, was extracted from ADNI [^{18}F]AV1451 scans. We performed linear models comparing [^{18}F]AV1451 signal across all 40 ROIs to Mini-Mental State Examination (MMSE) scores, adjusting for age, sex and education. **Results:** Significant relationships emerged only in two ROIs, both of which were data-driven. Inputting all regions plus demographics into a feature selection routine resulted in selection of three ROIs (two data-driven, one pathology-driven) and education, which together explained 25% of variance in MMSE scores. These results generalized to other tests of global cognition. **Interpretation:** Our findings suggest that hypothesis-free, data-derived ROIs may offer

enhanced clinical utility compared to theory-driven ROIs, by utilizing information specific to tau-PET signal.

INTRODUCTION

Alzheimer's disease (AD) is neuropathologically defined by the presence of widespread extracellular plaques containing amyloid-β and intracellular neurofibrillary tangles consisting of aggregated tau proteins [1,2]. While amyloid-β may be present decades prior to symptom onset [3], the presence of neocortical tau is temporally more closely related to current cognitive status and degree of neurodegeneration, as convincingly demonstrated by studies utilizing post-mortem tissue, animal models, cerebrospinal fluid and, more recently, the positron emission tomography (PET) tracer [^{18}F]AV1451 [4–9]. [^{18}F]AV1451 binds paired helical filaments of tau with high affinity and selectivity [10–14], and can be used to investigate the distribution of tau pathology in the living human brain. Several studies have shown strong spatial resemblance between *in vivo* tau PET patterns and neuropathological staging of neurofibrillary tangles as proposed by Braak and Braak [15–17], reflecting prototypical progression from (trans)entorhinal (stage I/II) to limbic (stage III/IV) to isocortical (stage V/VI) regions [1]. Furthermore, regional [^{18}F]AV1451 retention co-localizes with sites of brain atrophy or hypometabolism [7,18] and has been associated with impairments in specific cognitive domains [7–9].

Given this strong regional specificity of tau pathology, it is important to consider how regions-of-interest (ROIs) are defined, as they could potentially impact study outcomes. To date, most studies employing tau-PET tracers involved ROIs constructed

based on neuropathological studies. For example, some studies mimicked the Braak stages *in vivo* [15–17], while others selected specific regions reflecting early (e.g. entorhinal cortex) or more advanced (e.g. inferior temporal cortex) disease stages [19]. These approaches have several advantages as they are supported by fundamental research and enhance generalizability across studies. However, compared to neuroimaging, neuropathological data typically include only a few slices in a constrained number of brain regions, and brain tissue is affected by death and by the fact that it is non-living [20]. Additionally, tau PET signal does not equal presence of tau pathology. There are several sources of [^{18}F]AV1451 signal and noise, including target binding, off-target binding (e.g. Monamine oxidase, neuromelanin, vascular lesions, iron), non-specific binding and imaging related noise (e.g. partial volume effects) [14,12,15,21–25]. An alternative approach could therefore be to select ROIs based on data-driven approaches [26–28], thereby taking full advantage of the abundance of information contained in neuroimaging data, but also accounting the idiosyncrasies of PET imaging data.

In light of ongoing efforts to define appropriate ROIs and determine tau PET-positivity, it is important to compare data-driven approaches (agnostic, “where is the tau?”) with theory-derived ROIs based on post-mortem studies (directed, “is the tau here?”). In the present study, we applied an unsupervised algorithm to identify clusters of [^{18}F]AV1451 signal. We then compared the spatial patterns of these clusters with neuropathologically derived ROIs described in previous publications. Finally, we tested which ROI best correlated with global cognition in an independent cohort of cognitively normal, mild cognitive impairment and AD dementia subjects. We hypothesized that our

data-driven approach would corroborate neuropathological findings, but would also present novel information leading to enhanced associations with cognition.

MATERIALS AND METHODS

Participants

Two separate cohorts were included in this study. Participants from the Swedish BioFINDER study were used to perform clustering analysis on [^{18}F]AV1451 data, whereas participants from the Alzheimer's Disease Neuroimaging Initiative (ADNI) were used to test associations between the clustering-derived ROIs and cognition. Demographic, clinical and biomarker information for both cohorts are presented in Table 1.

The BioFINDER cohort is a multi-site study designed for the purpose of developing biomarkers for neurodegenerative diseases. More information can be found at http://biofinder.se. Study participants included 55 subjects with normal cognition, 21 with (MCI), and 47 with Alzheimer's dementia, who had complete MRI and [^{18}F]AV1451 PET data (Table 1). Patients with MCI were referred to a memory clinic and demonstrated objective cognitive impairment that could not be explained by another condition. AD dementia patients met criteria for the DSM-V [29] and NINCDS-ADRDA [30] for probable AD, established by clinicians blinded to PET data. To optimize overlap with the ADNI cohort, dementia patients were only included if they presented with an amnestic-predominant phenotype. Both dementia and MCI patients were only included in this study if they demonstrated abnormal Aβ1-42 levels in the CSF (INNOTEST, cut-off:

650 ng/l; Palmqvist *et al.*, 2015). The sample of controls selected for [^{18}F]AV1451 scanning was intentionally enriched for β-amyloid positivity to include people in the preclinical stage of AD (see Table 1). PET imaging for the study was approved by the Swedish Medicines and Products Agency and the local Radiation Safety Committee at Skåne University Hospital, Sweden. All participants provided written informed consent according to the Declaration of Helsinki, and ethical approval was given by the Ethics Committee of Lund University, Lund, Sweden.

Table 1: Demographic information, MMSE scores and amyloid-positivity rates

	Controls		**MCI**		**AD**		**Total**	
	BioF	**ADNI**	**BioF**	**ADNI**	**BioF**	**ADNI**	**BioF**	**ADNI**
n	55	43	21	37	47	10	123	90
Age (SD)	**75.0 (6.2)**	**70.3 (5.9)**	70.8 (10.9)	72.0 (6.8)	70.1 (8.6)	73.3 (4.3)	72.4 (8.4)	71.3 (6.1)
% Male	50.9%	46.5%	57.1%	67.6%	55.3%	60.0%	53.7%	56.7%
Education (SD)	**12.0 (3.7)**	**16.1 (2.4)**	**11.7 (3.7)**	**16.9 (2.7)**	**12.2 (3.2)**	**15.0 (3.0)**	**12.0 (3.5)**	**16.3 (2.6)**
% Amyloid+	43.6%	33.3%	**100%**	**44%**	100%	100%	**73.3%**	**44.8%**
MMSE (SD)	29.1 (1.1)	29.0 (1.3)	**25.7 (2.8)**	**28.4 (2.0)**	**21.2 (5.1)**	**25.5 (5.1)**	**25.5 (4.9)**	**28.3 (2.5)**

* **BOLD** text indicates significant difference ($p<0.05$) between cohorts, as measured by t-test, or Fisher's Exact Tests
ADNI = Alzheimer's Disease Neuroimaging Initiative; BioF = BioFINDER, MMSE = Mini-Mental State Examination; SD = Standard Deviation

ADNI is a multi-site open source dataset designed to accelerate the discovery of biomarkers to identify and track AD pathology [32]. The current study included all ADNI individuals with complete [^{18}F]AV1451 scans that were available in November, 2016. This included 43 cognitively normal elderly controls, 37 patients with MCI, and 10

patients with a recent diagnosis of Alzheimer's dementia (Table 1). In addition to imaging data, age, sex, education, diagnosis, amyloid-β status on [^{18}F]florbetapir PET [33], Mini-Mental State Examination (MMSE) [34] scores and other tests measuring global cognition or activities of daily living (see Table 2) were downloaded from the ADNI-LONI website (adni.loni.usc.edu).

Imaging

[^{18}F]AV1451 images were processed using separate but nearly identical pipelines across the two cohorts. Acquisition and processing procedures for [^{18}F]AV1451 processing in the BioFINDER cohort has been described elsewhere [35]. Scans were reconstructed into 5-min frames and motion corrected using AFNI's 3dvolreg https://afni.nimh.nih.gov/. Mean [^{18}F]AV1451 images were created over a time-window of 80-100 minutes post-injection, and these images were coregistered to each subject's T1 image in native space. Mean images were then intensity normalized using a complete cerebellar gray reference region to create standard uptake value ratio (SUVR) images. Coregistered MRI images were normalized to the MNI-ICBM152 template using Advanced Normalization Tools (https://stnava.github.io/ANTs/) and the transformation parameters were applied to the SUVR images. Finally, SUVR images were smoothed with an 8mm FWHM Gaussian filter.

For the ADNI cohort, mean 80-100 min [^{18}F]AV1451 images, as well as MPRAGE images closest to [^{18}F]AV1451 scans, were downloaded from the ADNI-LONI website. Details on acquisition procedures for these [^{18}F]AV1451 and MRI images can be found elsewhere (http://adni.loni.usc.edu/methods/documents/). [^{18}F]AV1451 images

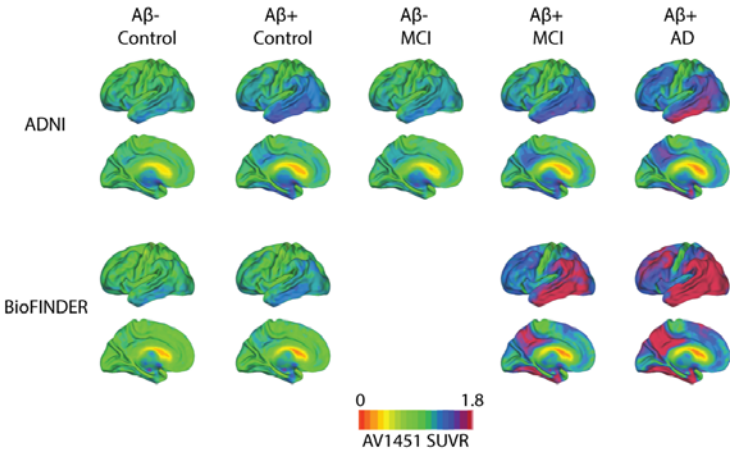

Figure 1. Mean [^{18}F]AV1451 uptake according to diagnosis, amyloid status and cohort
Mean [^{18}F]AV1451 SUVR images stratified by amyloid status and disease stage, across both the ADNI (top) and BioFINDER (bottom) cohorts.

were processed in accordance to procedures described in [15]. Briefly, T1 images were processed using Freesurfer v5.3 and [^{18}F]AV1451 images were coregistered to native T1s using Statistical Parametric Mapping 12 (www.fil.ion.ucl.ac.uk/spm/). SUVR images were created using a cerebellar gray reference region and images were normalized to MNI space using the parameters from the coregistered T1. Figure 1 shows mean [^{18}F]AV1451 SUVR images stratified by diagnosis and amyloid status for each cohort.

Clustering of [^{18}F]AV1451 data

Cross-subject [^{18}F]AV1451-PET covariance networks were derived from all 123 BioFINDER [^{18}F]AV1451 images using an open-source unsupervised consensus-clustering algorithm called Bootstrap Analysis of Stable Clusters (BASC; Figure 2) [36]. The algorithm was adapted to 3D [^{18}F]AV1451 data by stacking all 123 BioFINDER [^{18}F]AV1451 images along a fourth (subject) dimension, creating a single 4D image to be submitted as input. BASC first reduces the dimensions of the data with a previously described region-growing algorithm [37], which was set to extract spatially constrained atoms (small regions of redundant signal) with a size threshold of 1000mm^3. In order to

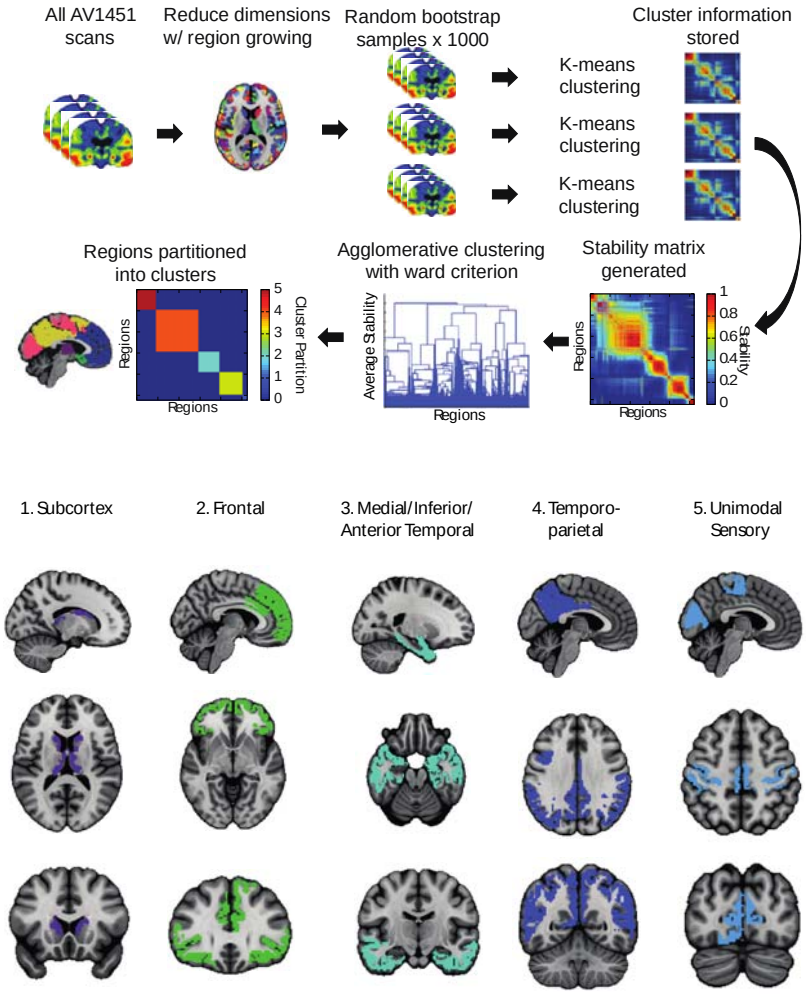

Figure 2. Bootstrap analysis of stable clusters on [^{18}F]AV1451 data. [^{18}F]AV1451 scans were entered into a voxelwise clustering algorithm. The optimal solutions were determined using the M-STEPS approach. This resulted in five [^{18}F]AV1451 covariance networks. These networks were masked with a stability threshold of 0.5, and are shown in the Figure above.

reduce computational demands, the Desikan-Killainy atlas [38] was used as a prior for region constraint, and the data was masked with a liberal gray matter mask, which included the subcortex but had the cerebellum manually removed (since this was used as the reference region for [^{18}F]AV1451 images). The region-growing algorithm resulted in a total of 730 atoms, which were included in the BASC algorithm. BASC next performs recursive k-means clustering on bootstrapped samples of the input data. After each clustering iteration, information about cluster membership is stored as a binarized adjacency matrix. The adjacency matrices are averaged resulting in a stability matrix representing probabilities of each pair of atoms clustering together (Figure 2). Finally, hierarchical agglomerative clustering with Ward criterion is applied to the stability ma trix, resulting in the final clustering solution. The

process is repeated over several clustering solutions (k=1 - 50), and the M-STEPs method [39] was implemented to find the most stable clustering solutions at different resolutions. In order to maintain relative similarity to Braak neuropathological staging (i.e. six ROIs), we chose the lowest resolution solution for subsequent analysis. Note that no size constraints were imposed on clustering solutions. Voxels were only included in a cluster when cluster probability membership exceed 0.5 (BASC default setting), eliminating unstable voxels from analysis [36,40]. After determining clusters in the BIOFINDER cohort, we extracted the (size-weighted) average [^{18}F]AV1451 SUVR for each cluster from all ADNI subjects, and these values were used for subsequent analysis investigating associations with cognition.

Definition of Braak stage ROIs described in other studies

A number of studies have created ROIs mirroring the Braak stages described from pathological studies. To test the utility of our data-driven ROIs vis-à-vis those defined in correspondence to the pathological literature, we recreated the Braak ROIs described in three different studies [15–17]. Schöll, Lockhart et al. and Cho et al. were constructed using regions from the Desikan-Killainy atlas, and we recreated these ROIs in direct correspondence to what has been reported in these two studies. Schwarz et al. instead generated small ROIs designed to mirror the slabs of cerebral cortex extracted during autopsy for Braak staging. These regions were constructed with a script generously provided by the authors. For all analyses, Braak ROIs were included both individually ("single") and cumulatively ("stage"). For example, for Braak Stage III, one ROI was created containing all regions from Braak I, II, and III included ("stage"), as well as a

ROI created including only regions in Braak III ("single"). Finally, some studies have chosen to use only the bilateral inferior temporal lobe from the Desikan-Killainy atlas to summarize global tau burden [19], so we included this region in subsequent analysis as well. Studies also frequently used the bilateral entorhinal cortex from this atlas, and it should be noted that this region is also included, namely as Stage I from Cho et al. and Schöll, Lockhart et al. Size-weighted average [^{18}F]AV1451 SUVR was extracted for each ROI (35 in total) for each subject.

Similarity between data-driven clusters, anatomical ROIs and Braak Stage ROIs

We compiled descriptive information about the similarity between our cluster-derived ROIs and the Braak ROIs from the literature. For comparisons to regions from Schöll, Lockhart et al. and Cho et al., we used normalized mutual information. Due to the small size of the Schwarz et al. regions, comparisons involved measuring the percentage of each Schwarz ROI falling inside of each cluster-derived ROI.

Statistical Analysis

In order to test the utility of our data-driven covariance networks, we performed linear models between these covariance networks and MMSE scores. The MMSE was chosen because it is a measure of global cognition, and because it is commonly employed in clinical practice, clinical trials and in many scientific studies. Separate general linear models for each ROI (40 in total; our five data-driven clusters and 35 ROIs from the literature) were constructed with MMSE score as the dependent variable and age, sex and

education as covariates. High collinearity was expected between ROIs so no multiple comparisons correction was performed. Rather, we aimed to establish whether regions generated from the clustering sample (BioFINDER) effectively described cognitive data in the test sample (ADNI), and whether it did so optimally in comparison to regions constructed based on pathological studies.

In order to identify a sparse set of non-redundant covariates that best describe the MMSE data in ADNI, we submitted all 40 tau ROIs plus age, sex and education to a Least Absolute Shrinkage and Selection Operator (Lasso) regression-based feature selection routine, implemented using scikit-learn [41] in Python 3.5.2 (https://www.python.org/). The Lasso uses an L1 regularization (coordinate descent) to penalize regression coefficients based on their maximum likelihood estimates, and is therefore an optimal approach to select a small number of variables from a large number of collinear covariates. In the current implementation, the degree of penalization (alpha parameter) is optimized using 10-fold cross-validation. All tau ROIs and demographics were scaled to be mean-centered with unit variance, and entered into the Lasso regression model with MMSE score as the dependent variable. Features selected by the Lasso (beta > 0.25) were entered together into a general linear model with MMSE as the dependent variable. Finally, to ensure our results were representative of global cognition and not specific to the MMSE, we repeated all of the previous analyses with several other tests of global cognition and function available in ADNI (see Table 2).

RESULTS

Participant Characteristics

Table 1 contains demographic information, MMSE scores and amyloid positivity rates for both the ADNI and BioFINDER sample. The sample used for clustering (BioFINDER) demonstrated important differences compared to the sample used for testing (ADNI). BioFINDER subjects were less highly educated across the whole sample, and BioFINDER controls were on average older than ADNI controls. Additionally, the BioFINDER sample demonstrated lower MMSE scores across the whole sample compared to ADNI, including within MCI and dementia groups. Finally, 45% of ADNI subjects were amyloid-positive vs. 73% of BioFINDER subjects, which was primarily related to the fact that only amyloid positive MCI patients were included in the BioFINDER sample.

Data-driven Tau-PET covariance networks

123 BioFINDER [^{18}F]AV1451 scans were entered into an advanced clustering algorithm in order to identify networks of regional [^{18}F]AV1451 signal covariance across subjects. The M-STEPS algorithm identified five-, nine- and 32-cluster solutions as optimal solutions. For the purposes of comparing with Braak stage ROIs, we chose the lowest-resolution solution (n=5) for subsequent analyses, visualized in Figure 2. The clusters were interpreted and named as follows: “1: Subcortical”, “2: Frontal”, “3: Medial/Anterior/Inferior Temporal”, “4: Temporo-parietal” and “5: Unimodal Sensory”. Cluster 3 bore resemblance to regions often involved in early tau aggregation and atrophy [1], while Cluster 4 also appeared similar to regions commonly associated with neurodegeneration in AD [26,27]. Of note, the hippocampus was largely unrepresented in any of the cluster-cores, though some voxels in the head of the hippocampus were

included in Cluster 3, and a few distributed voxels were included in Cluster 1 (Subcortex). However, using a winner-takes-all clustering approach, most of the hippocampus clustered with other subcortical and periventricular regions.

Similarity to Braak ROIs

Descriptive metrics were used to quantify the spatial similarity between the data-driven covariance networks and the Braak Stage ROIs introduced in the literature (Figure 3). Cluster 5 ("Unimodal Sensory") demonstrated a high degree of overlap with Braak Stage VI across all region sets. Spatial similarity was also evident between Cluster 3 ("Medial/Anterior/Inferior Temporal") and Stage I-IV from Cho et al., and this cluster almost completely circumscribed Stages I-III from Schwarz et al. Cluster 1 ("Subcortex") was most similar to Schöll, Lockhart et al. Stage II, due in part to its inclusion of the hippocampus. Little spatial similarity was evident between Cluster 2 ("Frontal") and any of the Braak Stage ROIs, though some similarity was seen with the Stage V region from Schöll, Lockhart et al. and Cho et al. due to their inclusion of many frontal lobe structures. Similarly, Cluster 4 ("Temporo-parietal") did not demonstrate strong spatial similarity to any of the Braak ROIs, though it did partially overlap with the Braak Stage VI and Stage V regions from Schwarz et al.

Associations with global cognition in ADNI

General linear models were run in the ADNI dataset assessing associations separately between each of 40 tau ROIs (our five data-driven clusters established in the

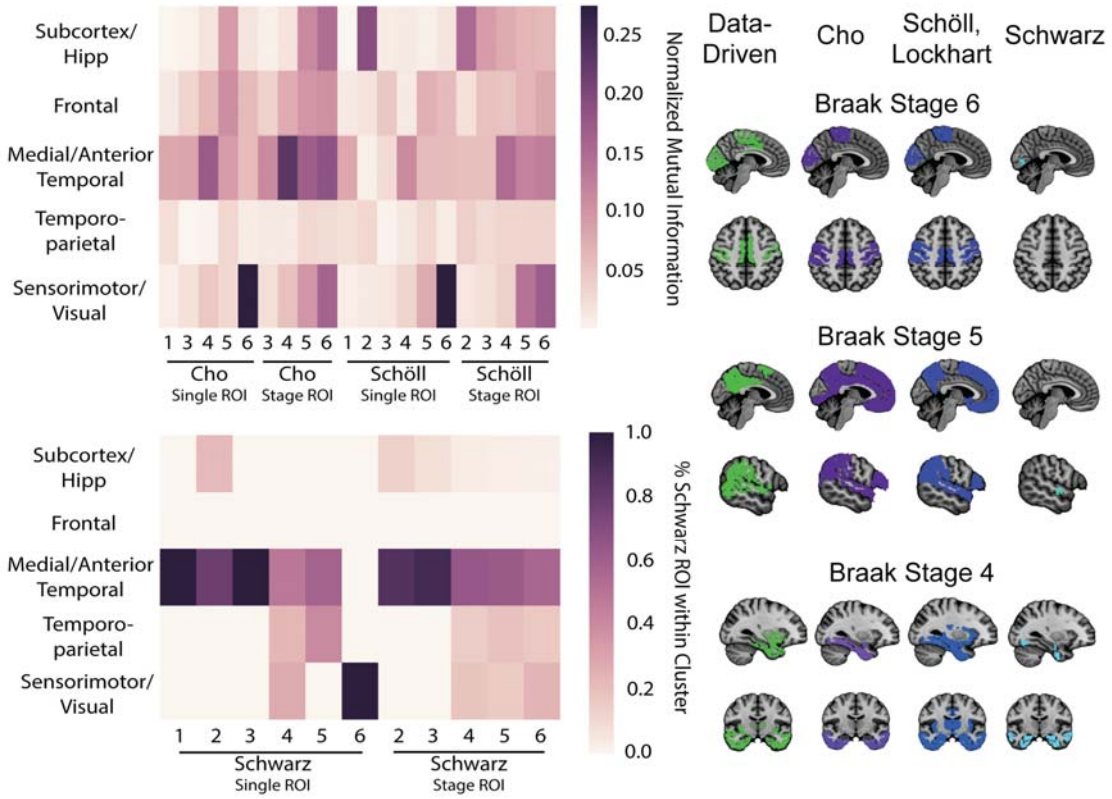

Figure 3. Comparison between data-driven and hypothesis-driven ROIs. Data-driven [^{18}F]AV1451 covariance networks were compared to previously existing Braak Stage ROIs from the literature using descriptive statistics. The clusters were compared to ROIs from Schöll, Lockhart et al. and Cho et al using Normalized Mutual Information (top left), and were compared to regions from Schwarz et al. using the percentage of Schwarz ROI voxels within each data-driven cluster.

BioFINDER study, and 35 ROIs from the literature) and MMSE scores, controlling for age, sex and education. Uncorrected effect sizes can be found in Figure 4. The highest effect sizes were seen with Cluster 4 ("Temporo-parietal"; β = -3.27 [SE=1.33], t = -2.45, p=0.016) and Cluster 3 ("Medial/Anterior/Inferior Temporal"; β = -2.75 [SE=1.37], t = -2.00, p=0.049). Only these two ROIs met the uncorrected threshold for significance, while several others reach trend level of significance (Figure 4).

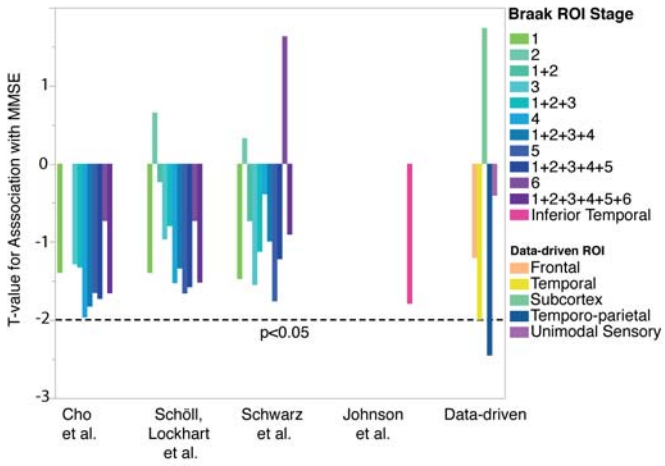

FIGURE 4. Associations between [^{18}F]AV1451 ROIs and MMSE scores. General linear models comparing [^{18}F]AV1451 signal to MMSE were run, adjusting for age, sex and education. For each model, a different [^{18}F]AV1451 ROI was used. ROIs included the five clusters identified in our analysis, as well as Braak stage regions taken from three different papers: Schöll, Lockhart et al., 2016 *Neuron*; Cho et al., 2016 *Ann. Neurol.*; Schwarz et al., 2016 *Brain*. Two versions of each Braak ROIs were created, one using regions from that stage only (e.g. Stage 3), and one combining all regions from that stage with all regions from previous stages (e.g. Stage 1+2+3). The effect size (t-value) of each tau ROI is shown. Only the data-driven Medial/Inferior Temporal region and Temporo-parietal region demonstrate significant relationships with MMSE.

Next, all tau ROIs were entered into a Lasso regression model in order to identify a sparse set of covariates that best describe the MMSE data (Figure 5). The optimal penalization value was defined through cross-validation as 2.11. The Lasso reduced all coefficients to zero except Cluster 4 ("Temporo-parietal"), Cluster 1 ("Subcortical"), Braak Stage VI from Schwarz et al., and education. These four variables were entered together into a general linear model, and together explained a much greater proportion of variance in MMSE data (r^2[4:81] = 0.25, p<0.0001; Figure 5) compared to the individual effect sizes of each covariate (highest r^2 = 0.064; see Table 2). The earlier negative association between Cluster 4 and MMSE was strengthened (t=-3.86, p<0.001), although positive associations were seen for the other three covariates (Cluster 1: t = 1.43, p = 0.15; Schwarz Single 6: t = 3.24, p = 0.002; Education: t = 2.53, p = 0.049).

Sensitivity analyses

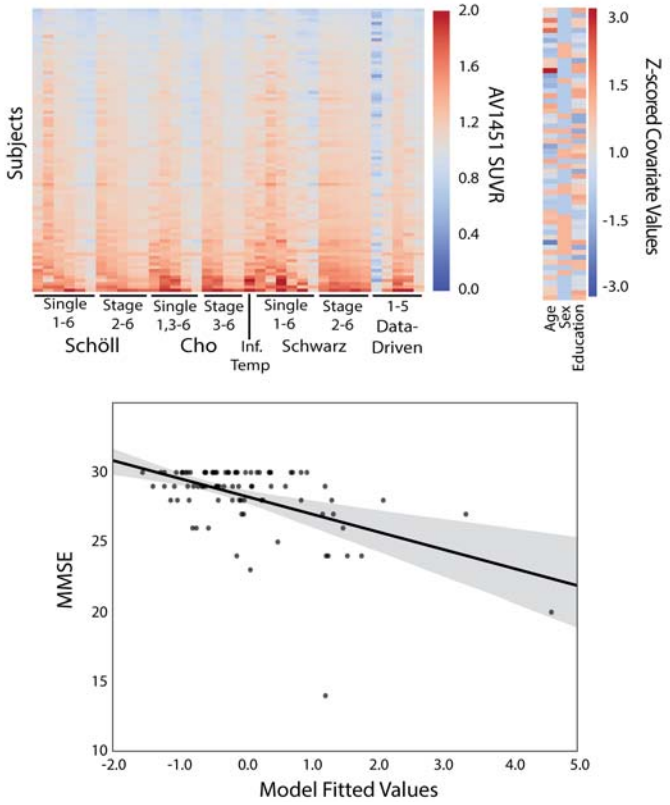

FIGURE 5. Lasso regression selects data-driven ROIs. All [^{18}F]AV1451 ROIs plus age, sex and education were entered into a L1-penalized Lasso regression feature selection routine. The Lasso selected education and three ROIs: the data-driven Temporo-parietal region, data-driven subcortical region and the Schwarz Single VI region. Together, these features explained 25% of the variance in MMSE data.

To ensure our results were not specific to the MMSE, we repeated this analysis using five other measures of global cognition and function available in ADNI. The data-driven Cluster 4 ("Temporo-parietal") described global cognition better than all other ROIs using three of the five cognitive measures, and was in the top five for all of them (Table 2). Across all cognitive measures, Clusters 4 and 3 ("Medial/anterior/inferior temporal") ranked best and second best respectively at describing global cognitive data (Figure 6). Notably, the Schwarz Stage I ROI also performed quite well across cognitive measures, except for the MMSE. The Lasso analysis was also repeated for the other five tests of global cognition. The data-driven Cluster 4 was selected across all six analyses, and was the only ROI selected for two analyses (data not shown).

DISCUSSION

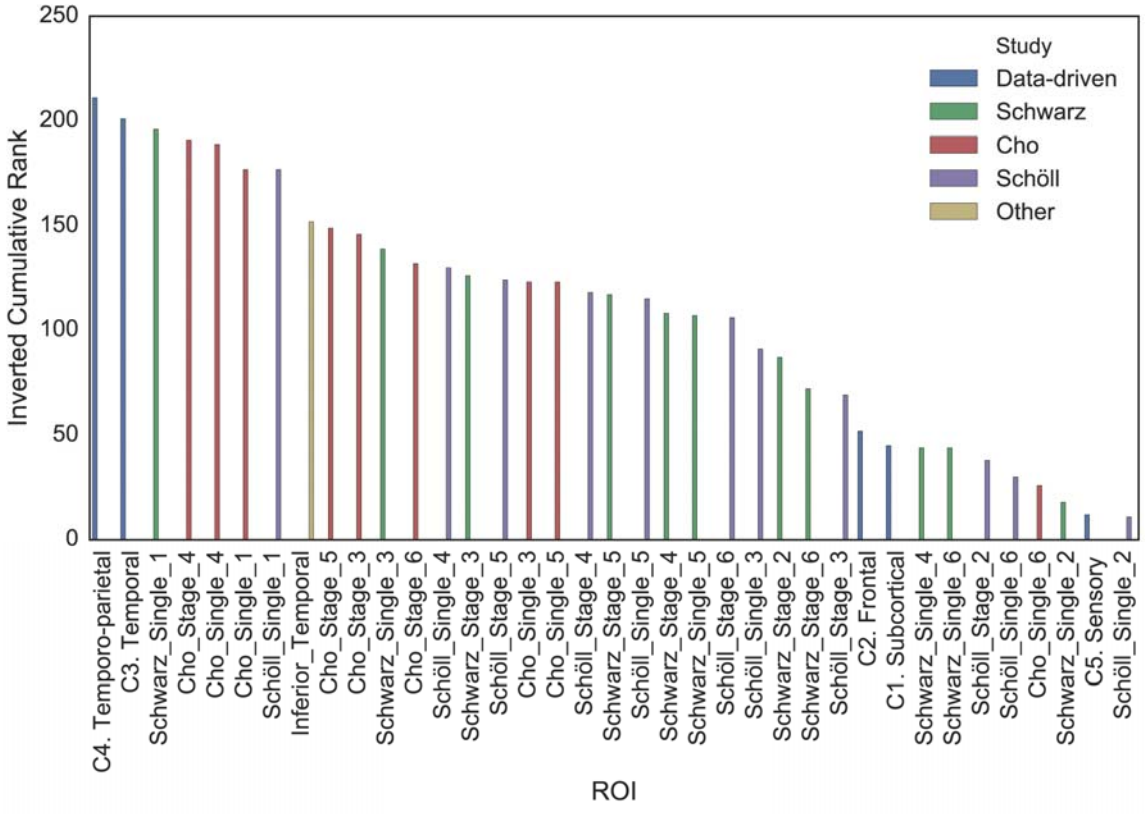

Figure 6. Cumulative ranking of ROI performance across all measures of global cognition and function. For each measure of global cognition (see Table 2), [^{18}F]AV1451 ROIs were ranked from worst to best (such that the worst region would have rank of 1) with respect to the effect size of the association between [^{18}F]AV1451 in that region and the cognitive score. The ranks were then summed across all cognitive measurements and are displayed here. The data-driven Cluster 4 ("Temporo-parietal") ranked the best cumulatively across cognitive tests, with the data-driven Cluster 3 ("Medial/Inferior/Anterior temporal") ranking second best.

In the present study, we applied an advanced unsupervised algorithm to identify clusters of [^{18}F]AV1451 signal in 123 subjects ranging from cognitively normal to AD dementia in the Swedish BioFINDER study. Our approach yielded clusters in the temporoparietal, medial/inferior/anterior temporal, unimodal sensory and frontal cortex, as well as the subcortex. In an independent sample of 90 subjects (ADNI), we performed general linear models between tests of global cognition and each [^{18}F]AV1451 cluster, adjusting for

age, sex and education. In addition, we ran similar models using 35 neuropathologically derived ROIs from previous publications [15–17,19].

Table 2. Best-ranking AV1451 ROIs at describing global cognition across different cognitive tests

MMSE[a]

Rank	Study	ROI	t
1	Data-driven	Temporo-parietal	-2.45*
2	Data-driven	Temporal	-2.00*
3	Cho	Single IV	-1.97
4	Cho	Stage IV	-1.83
5	Other	Inferior Temporal	-1.80

CDRSBb

Study	ROI	t
Schwarz	Stage I	3.60***
Data-driven	Temporo-parietal	3.49***
Cho/Scholl	Stage I	3.49***
Data-driven	Temporal	3.33***
Cho	Stage IV	3.18***

ADAS11[c]

Rank	Study	ROI	t
1	Data-driven	Temporo-parietal	4.10***
2	Schwarz	Stage I	3.50***
3	Cho	Single IV	3.43***
4	Data-driven	Temporal	3.39**
5	Cho	Stage IV	3.33**

ADAS13[d]

Study	ROI	t
Data-driven	Temporo-parietal	3.02**
Schwarz	Stage I	2.57*
Data-Driven	Temporal	2.35*
Cho/Scholl	Stage I	2.34*
Cho	Single IV	2.34*

ECOG[e]

Rank	Study	ROI	t
1	Data-driven	Temporo-parietal	3.68**
2	Cho	Stage IV	3.48**
3	Schwarz	Stage I	3.40*
4	Cho	Single IV	3.40*
5	Data-Driven	Temporal	3.40*

FAQ[f]

Study	ROI	t
Schwarz	Stage I	2.91**
Data-driven	Temporal	2.69**
Cho/Scholl	Stage I	2.68**
Data-driven	Temporo-parietal	2.67**
Cho	Stage III	2.63*

* p<0.05 ** p<0.01 *** p<0.001

MMSE = Mini-Mental State Examination; CDRSB = Clinical Dementia Rating Sum of Boxes; ADAS = Alzheimer's disease Assessment Scale; ECog = Everyday Cognition; FAQ = Functional Activities Questionnaire

a 34, b 51, c 52, d 53, e 54, f 55

Across all ROIs, only two were significantly associated with MMSE score, and they were both data-driven clusters (temporoparietal and medial/inferior/anterior temporal cortex). In addition, the temporoparietal data-driven cluster was among the most important features (identified by a Lasso regression model) for predicting MMSE scores. These findings were generalizable to other measures of global cognition and function. Unsupervised clustering of [^{18}F]AV1451 PET data thus revealed ROIs resembling well described vulnerable regions in AD, which enhanced description of cognitive data in an independent dataset. This suggests that data-driven approaches to delineate ROIs may improve clinical utility of [^{18}F]AV1451 PET data.

The tau-PET covariance networks derived from our clustering approach exhibited a fair degree of overlap with Braak ROIs derived from autopsy studies, thereby demonstrating biological relevance. Particularly, Cluster 3 ("Medial/Anterior/Inferior Temporal") was reminiscent of regions involved in early tau accumulation, whereas Cluster 5 ("Unimodal Sensory") demonstrated a high degree of similarity to regions involved only in the latest stages of AD. In contrast, Cluster 4 ("Temporo-parietal") did not strongly resemble any of the Braak regions, while its pattern, together with the pattern of cluster 3, spatially overlapped with cortical regions most vulnerable to neurodegeneration in AD [26,27]. Furthermore, signal in the hippocampus was heterogenous, adding additional evidence that [^{18}F]AV1451 signal in this structure should be interpreted with caution [17 21,24]. Similarly, our data-driven approach suggested that most (but not all) frontal lobe structures exhibited [^{18}F]AV1451 signal patterns unique to the rest of the cortex. This is notable considering the original Braak Stage V aggregates frontal lobe structures with many of the temporo-parietal structures captured in our

Cluster 4. Part of the successful description of cognitive data by the data-driven ROI may be due to its isolation from many of these frontal lobe structures, which may be contributing signal less informative to AD progression, particularly in early disease stages. Finally, our data-driven ROIs provide information that may reconcile some differences between existing Braak ROIs. For example, in our study, [^{18}F]AV1451 signal in the putamen and insula covaried with other regions involved in early tau accumulation, which was similar to the ROIs described by Schöll, Lockhart et al., but not Cho et al.

Despite the clusters being derived from a sample with several important and disease-relevant differences compared to the testing sample, these data-driven ROIs described global cognitive data better than regions derived from autopsy studies. While the improvement over the other regions was subtle, the increasing movement toward the development of biomarkers demands optimization of ROIs to summarize [^{18}F]AV1451 signal [42–44]. As such, even small improvements are important for studies assessing more subtle effects of cortical tau accumulation and studies seeking optimal biomarkers for multimodal classification or disease progression [45]. The improvement observed is likely due to the data-driven nature of the method used for derivation of the clusters. [^{18}F]AV1451 may be binding to several off-target agents, such as (neuro)melanin, iron, vascular pathology and MAO-A/B [14,12,21,22], and as such, [^{18}F]AV1451 signal is likely a mix of true tau pathology and other off-target and non-specific signals. Deriving the clusters from a sample representing a wide breadth of disease stages and additionally including subjects unlikely to have significant cortical tau pathology enhances the likelihood of isolating true tau signal, which covaries strongly and in a regionally specific pattern across disease stages. Additionally, deriving the clusters voxelwise allows

freedom from anatomical borders, which may impose unnecessary constraints irrelevant to the spread of tau. Finally, despite its many limitations, multi-subject automatic whole-brain sampling is a distinct advantage of [^{18}F]AV1451-PET over pathological studies. This advantage may further enhance the efficacy of data-driven approaches to ROI generation, which evaluate regions equally that may otherwise be overlooked.

The results of this study thus suggest a possible advantage of data-driven approaches in evaluating [^{18}F]AV1451 PET data as a biomarker for AD. This study adds to a rapidly growing body of data-driven [^{18}F]AV1451-PET studies that have helped to characterize features of this tracer in the context of AD. Sepulcre and colleagues employed a similar unsupervised clustering approach on a set of cognitively intact elderly individuals, which, similar to our study, revealed [^{18}F]AV1451-PET covariance between regions of early- and later- stage tau accumulation [46]. This suggests these patterns of signal covariance are stable even in the earliest disease stages, lending credence to the use of data-driven biomarkers in multiple contexts. Meanwhile, Jones et al. used a data-driven Independent Components Analysis approach to summarize [^{18}F]AV1451 data [47]. While the authors concluded the resulting ROIs represented functional brain networks, three of the ROIs bore a striking similarity to those generated by our clustering approach. Our approach builds on these previous studies by assessing relationships between data-driven ROIs and cognition, and by comparing them with other existing ROIs. Maass et al. employed a series of *a priori* and supervised data-driven methods to generate [^{18}F]AV1451 ROIs and found a relative equivalence between these ROIs in their association with cognition and a number of other disease markers [43]. However, consistent with our study, Maass et al. found [^{18}F]AV1451 signal to covary most strongly within a

specific set of AD vulnerable-regions, and conclude that these regional measures may perform better than whole-brain ROIs, particularly regarding associations with cognition.

We employed a widely used feature selection routine to identify those regions most informative in describing association between [^{18}F]AV1451 signal and cognitive data. The feature most strongly associated with MMSE was the data-driven temporo-parietal cluster, which harbored a strong negative relationship when included with the other selected features ($p<0.001$). However, the feature selection also resulted in the selection of somewhat unexpected features, namely the data-driven Cluster 1 ("Subcortex"), Schwarz et al. Stage VI and education, all of which associated positively with MMSE in a general linear model. The finding of an association between education and MMSE controlling for tau pathology is consistent with the concept of cognitive reserve [48], and suggests that more highly educated subjects may experience preserved cognition in the face of tau pathology [49]. While the selection of Cluster 1 and Schwarz Stage VI are less obvious, possible explanations include partial volume effects and age-related off-target or non-specific signal. Because very few ADNI subjects demonstrate strong [^{18}F]AV1451 signal in either of these ROIs, higher [^{18}F]AV1451 signal may be related to the presence of more cortex (and thus more off-target or non-specific binding) rather than increased tau pathology. Similarly, off-target [^{18}F]AV1451 signal in the cortex and subcortex has been shown to increase with age [15,21,50], possibly representing binding to reactive astrocytes [25] or iron deposits [21]. Since age was not selected by the Lasso and therefore was not included in the multivariate model, this may explain the positive association between these regions and MMSE. However, the fact that these ROIs were selected instead of age suggests they may carry additional cognition-relevant

information, which may demand further exploration. Regardless, the negative relationship between Cluster 4 ("Temporo-parietal") and MMSE was substantially increased after regressing out these "noisy" variables. This suggests that [^{18}F]AV1451-cognition relationships may be enhanced by regressing out off-target or non-specific signal sources.

Our study comes with a number of limitations. First, there were several differences in characteristics between the two samples. We decided to use the BioFINDER cohort for clustering given the broad range of both [^{18}F]AV1451 uptake (Figure 1) and MMSE scores (Table 1). As a consequence, validation of the clusters was performed in subjects from the ADNI cohort with more restricted [^{18}F]AV1451 uptake and cognitive scores. Second, in the trade-off between precise psychometric tracing of cognition and use of simpler but widely available tests, we selected a rather crude outcome measure for cognition (i.e. MMSE) to enhance reproducibility of our results. We partially addressed this concern by validating our results with other available measures of global cognition. Third, contrary to other studies, we did not make an attempt to classify individuals according to stages of tau pathology. Finally, we chose not to apply partial volume correction on our data. Investigating the impact of such corrections is certainly important, but we were interested in the natural behavior of tau-PET signal before any corrections.

In order to aid future studies, we have made the [^{18}F]AV1451 clusters from this study available on FigShare (doi = 10.6084/m9.figshare.5758374).

Acknowledgements

Work at the authors' research centers was supported by the European Research Council, the Swedish Research Council, the Strategic Research Area MultiPark (Multidisciplinary Research in Parkinson's disease) at Lund University, the Swedish Brain Foundation, the Swedish Alzheimer Association, the Marianne and Marcus Wallenberg Foundation, the Skåne University Hospital Foundation, and the Swedish federal government under the ALF agreement. This research was additionally funded by Marie Curie FP7 International Outgoing Fellowship [628812] (to R.O.); The donors of [Alzheimer's Disease Research], a program of BrightFocus Foundation (to R.O.); Author JWV was additionally funded by an Alzheimer Nederland grant and a Vanier Canada Graduate Studies Doctoral award. The authors would like to thank Emma Wolters, Tessa Timmers, Colin Groot, Angela Tam, Alle Meije Wink and Elena Kochova for advice and support. The authors would additionally like to thank Adam Schwarz for providing scripts to recreate the ROIs from Schwarz et al., 2016, and Chul Hyoung Lyoo for providing information about creating ROIs from Cho et al., 2016. AVID Radiopharmaceutical generously provided the precursor of AV-1451. Data collection and sharing for this project was funded in part by the Alzheimer's Disease Neuroimaging Initiative (ADNI) (National Institutes of Health Grant U01 AG024904) and DOD ADNI (Department of Defense award number W81XWH-12-2-0012). ADNI is funded by the National Institute on Aging, the National Institute of Biomedical Imaging and Bioengineering, and through generous contributions from the following: AbbVie, Alzheimer's Association; Alzheimer's Drug Discovery Foundation; Araclon Biotech; BioClinica, Inc.; Biogen; Bristol-Myers Squibb Company; CereSpir, Inc.; Eisai Inc.; Elan Pharmaceuticals, Inc.; Eli Lilly and Company; EuroImmun; F. Hoffmann-La Roche Ltd and its affiliated company Genentech, Inc.; Fujirebio; GE Healthcare; IXICO Ltd.; Janssen Alzheimer Immunotherapy Research & Development, LLC.; Johnson & Johnson Pharmaceutical Research & Development LLC.; Lumosity; Lundbeck; Merck & Co., Inc.; Meso Scale Diagnostics, LLC.; NeuroRx

Research; Neurotrack Technologies; Novartis Pharmaceuticals Corporation; Pfizer Inc.; Piramal Imaging; Servier; Takeda Pharmaceutical Company; and Transition Therapeutics. The Canadian Institutes of Health Research is providing funds to support ADNI clinical sites in Canada. Private sector contributions are facilitated by the Foundation for the National Institutes of Health (www.fnih.org). The grantee organization is the Northern California Institute for Research and Education, and the study is coordinated by the Alzheimer's Disease Cooperative Study at the University of California, San Diego. ADNI data are disseminated by the Laboratory for Neuro Imaging at the University of Southern California

Author Contributions

J.W.V. and R.O. conceptualized and designed the study. P.S., A.C.E., O.H. and R.O. supervised the study. J.W.V., N.M., Y.I.M., T.O.S., M.S., P.B., O.H. and R.O. acquired, processed and analyzed the data. J.W.V., W.F. and R.O. drafted the manuscript. All authors provide critical or conceptual support and revised the manuscript.

Potential Conflicts of Interest

OH has acquired research support (for the institution) from Roche, GE Healthcare, Biogen, AVID Radiopharmaceuticals, Fujirebio, and Euroimmun. In the past 2 years, he has received consultancy/speaker fees (paid to the institution) from Lilly, Roche, and Fujirebio. Many of these companies are involved in creating tau-PET radioligands, including AVID, who provided the ligands for this study.

1. Braak H, Braak E. Neuropathological stageing of Alzheimer-related changes. Acta Neuropathol. 1991;82(4):239–59.
2. Masters CL, Simms G, Weinman NA, et al. Amyloid plaque core protein in Alzheimer disease and Down syndrome. Proc. Natl. Acad. Sci. U. S. A. 1985;82(12):4245–9.
3. Jansen WJ, Ossenkoppele R, Knol DL, et al. Prevalence of Cerebral Amyloid Pathology in Persons Without Dementia: A Meta-analysis. JAMA 2015;313(19):1924–1938.
4. Arriagada P V, Growdon JH, Hedleywhyte ET, Hyman BT. Neurofibrillary Tangles But Not Senile Plaques Parallel Duration and Severity of Alzheimers-Disease. Neurology 1992;42(3):631–639.
5. Nelson P. T. et al. Correlation of Alzheimer Disease Neuropathologic Changes With Cognitive Status: A Review of the Literature. J Neuropathol Exp Neurol. 2012 May□; 71(5) 362–381.
6. Van Rossum IA, Visser PJ, Knol DL, et al. Injury markers but not amyloid markers are associated with rapid progression from mild cognitive impairment to dementia in alzheimer's disease. J. Alzheimer's Dis. 2012;29(2):319–327.
7. Ossenkoppele R, Schonhaut DR, Schöll M, et al. Tau PET patterns mirror clinical and neuroanatomical variability in Alzheimer's disease Brain 2016;139(5):1551–1567.
8. Cho H, Choi JY, Lee SH, et al. Excessive tau accumulation in the parieto-occipital cortex characterizes early-onset Alzheimer's disease. Neurobiol. Aging 2017;53:103–111.
9. Bejanin A, Schonhaut DR, Joie R La, et al. Tau pathology and neurodegeneration contribute to cognitive impairment in Alzheimer's disease. Brain 2017;140(12):3286-3300
10. Chien DT, Bahri S, Szardenings AK, et al. Early Clinical PET Imaging Results with the Novel PHF-Tau Radioligand [F-18]-T807. J. Alzheimer's Dis. 2013;34(2):457–468.
11. Xia C-F, Arteaga J, Chen G, et al. [18F]T807, a novel tau positron emission tomography imaging agent for Alzheimer's disease. Alzheimer's Dement. 2013;9(6):666–676.
12. Lowe VJ, Curran G, Fang P, et al. An autoradiographic evaluation of AV-1451 Tau PET in dementia. Acta Neuropathol. Commun. 2016;4(1):58.
13. Marquié M, Siao Tick Chong M, Antón-Fernández A, et al. [F-18]-AV-1451 binding correlates with postmortem neurofibrillary tangle Braak staging. Acta Neuropathol. 2017;134(4):619-628.
14. Marquié M, Normandin MD, Vanderburg CR, et al. Validating novel tau positron emission tomography tracer [F-18]-AV-1451 (T807) on postmortem brain tissue. Ann. Neurol. 2015;78(5):787–800.
15. Schöll M, Lockhart SN, Schonhaut DR, et al. PET Imaging of Tau Deposition in the Aging Human Brain. Neuron 2016;89(5):971–982.
16. Schwarz AJ, Yu P, Miller BB, et al. Regional profiles of the candidate tau PET ligand ^{18} F-AV-1451 recapitulate key features of Braak histopathological stages. Brain 2016;139(5):1539-1550
17. Cho H, Choi JY, Hwang MS, et al. In vivo cortical spreading pattern of tau and

amyloid in the Alzheimer's disease spectrum. Ann. Neurol. 2016;80(2):247-258

18. Xia C, Makaretz SJ, Caso C, et al. Association of In Vivo [^{18} F]AV-1451 Tau PET Imaging Results With Cortical Atrophy and Symptoms in Typical and Atypical Alzheimer Disease. JAMA Neurol. 2017;74(4):427.
19. Johnson KA, Schultz A, Betensky RA, et al. Tau positron emission tomographic imaging in aging and early Alzheimer disease. Ann. Neurol. 2016;79(1):110–119.
20. Scheltens P, Rockwood K. How golden is the gold standard of neuropathology in dementia? Alzheimer's Dement. 2011;7(4):486–489
21. Choi JY, Cho H, Ahn SJ, et al. "Off-Target" ^{18} F-AV-1451 Binding in the Basal Ganglia Correlates with Age-Related Iron Accumulation. J. Nucl. Med. *In Press*
22. Ng KP, Pascoal TA, Mathotaarachchi S, et al. Monoamine oxidase B inhibitor, selegiline, reduces 18 F-THK5351 uptake in the human brain. Alzheimers. Res. Ther. 2017;9(1):25.
23. Lockhart SN, Ayakta N, Winer JR, et al. Elevated (18)F-AV-1451 PET tracer uptake detected in incidental imaging findings. Neurology 2017;88(11):1095–1097.
24. Ikonomovic MD, Abrahamson EE, et al. [F-18] AV-1451 PET retention in choroid plexus : more than " off-target " binding. Ann. Neurol. 2016;80(2):307-308.
25. Harada R, Ishiki A, Kai H, et al. Correlations of (18)F-THK5351 PET with post-mortem burden of tau and astrogliosis in Alzheimer's disease. J. Nucl. Med. *In Press*
26. Landau SM, Harvey D, Madison CM, et al. Associations between cognitive, functional, and FDG-PET measures of decline in AD and MCI. Neurobiol. Aging 2011;32(7):1207–1218.
27. Dickerson BC, Stoub TR, Shah RC, et al. Alzheimer-signature MRI biomarker predicts AD dementia in cognitively normal adults. Neurology 2011;76(16):1395–1402.
28. Pankov A, Binney RJ, Staffaroni AM, et al. Data-driven regions of interest for longitudinal change in frontotemporal lobar degeneration. NeuroImage Clin. 2016;12:332–340.
29. American Psychiatric Association T. Diagnostic and statistical manual of mental disorders : DSM-5. Fifth edition. Arlington, VA : American Psychiatric Association. 2013
30. McKhann G, Knopman DS, Chertkow H, et al. The diagnosis of dementia due to Alzheimer's disease: Recommendations from the National Institute on Aging-Alzheimer's Association workgroups on diagnostic guidelines for Alzheimer's disease. Alzheimers Dement. 2011;7(3):263–269.
31. Palmqvist S, Zetterberg H, Mattsson N, et al. Detailed comparison of amyloid PET and CSF biomarkers for identifying early Alzheimer disease. Neurology 2015;85(14):1240–1249.
32. Weiner MW, Veitch DP, Aisen PS, et al. The Alzheimer's disease neuroimaging initiative: A review of papers published since its inception. Alzheimer's Dement. 2012;8(1 SUPPL.):S1–S68.
33. Landau SM, Lu M, Joshi AD, et al. Comparing positron emission tomography imaging and cerebrospinal fluid measurements of β-amyloid. Ann. Neurol.

2013;74(6):826–836.
34. Folstein MF, Folstein SE, McHugh PR. “Mini-mental state”. A practical method for grading the cognitive state of patients for the clinician. J. Psychiatr. Res. 1975;12(3):189–98.
35. Hansson O, Grothe MJ, Strandberg TO, Ohlsson T. Tau Pathology Distribution in Alzheimer ’ s disease Corresponds Differentially to Cognition-Relevant Functional Brain Networks. 2017;11(March)
36. Bellec P, Rosa-Neto P, Lyttelton OC, et al. Multi-level bootstrap analysis of stable clusters in resting-state fMRI. Neuroimage 2010;51(3):1126–1139.
37. Bellec P, Perlbarg V, Jbabdi S, et al. Identification of large-scale networks in the brain using fMRI. Neuroimage 2006;29(4):1231–1243.
38. Desikan RS, Ségonne F, Fischl B, et al. An automated labeling system for subdividing the human cerebral cortex on MRI scans into gyral based regions of interest. Neuroimage 2006;31(3):968–980.
39. Bellec P. Mining the hierarchy of resting-state brain networks: Selection of representative clusters in a multiscale structure. Proc. - 2013 3rd Int. Work. Pattern Recognit. Neuroimaging, PRNI 2013 2013;54–57.
40. Garcia-Garcia M, Nikolaidis A, Bellec P, et al. Detecting stable individual differences in the functional organization of the human basal ganglia. Neuroimage *In Press*
41. Pedregosa F, Varoquaux G, Gramfort A, et al. Scikit-learn: Machine Learning in Python [Internet]. J. Mach. Learn. Res. 2012;12:2825–2830.
42. Frisoni GB, Boccardi M, Barkhof F, et al. Strategic roadmap for an early diagnosis of Alzheimer’s disease based on biomarkers. Lancet. Neurol. 2017;16(8):661–676.
43. Maass A, Landau S, Baker SL, et al. Comparison of multiple tau-PET measures as biomarkers in aging and Alzheimer ’ s disease. Neuroimage 2017;157:448–463.
44. Mishra S, Gordon BA, Su Y, et al. AV-1451 PET imaging of tau pathology in preclinical Alzheimer disease: Defining a summary measure. Neuroimage 2017;161:171–178.
45. Ota K, Oishi N, Ito K, Fukuyama H. Effects of imaging modalities, brain atlases and feature selection on prediction of Alzheimer’s disease. J. Neurosci. Methods 2015;256:168–183.
46. Sepulcre J, Grothe MJ, Sabuncu M, et al. Hierarchical Organization of Tau and Amyloid Deposits in the Cerebral Cortex. JAMA Neurol. 2017;74(7):813.
47. Jones DT, Graff-Radford J, Lowe VJ, et al. Tau, Amyloid, and Cascading Network Failure across the Alzheimer’s disease Spectrum. Cortex 2017;97:143-159.
48. Stern Y. Cognitive reserve in ageing and Alzheimer’s disease. Lancet Neurol. 2012;11(11):1006–1012.
49. Hoenig MC, Bischof GN, Hammes J, et al. Tau pathology and cognitive reserve in Alzheimer’s disease. Neurobiol. Aging 2017;57:1–7.
50. Smith R, Schain M, Nilsson C, et al. Increased Basal Ganglia Binding of 18F-AV-1451 in Patients With Progressive Supranuclear Palsy. Mov. Disord. 2016;0(0):1–7.
51. Hughes CP, Berg L, Danziger WL, et al. A new clinical scale for the staging of dementia. Br. J. Psychiatry 1982;140:566–72.
52. Mohs RC, Knopman D, Petersen RC, et al. Development of cognitive instruments

for use in clinical trials of antidementia drugs: additions to the Alzheimer's Disease Assessment Scale that broaden its scope. The Alzheimer's Disease Cooperative Study. Alzheimer Dis. Assoc. Disord. 1997;11 Suppl 2:S13-21.

53. Rosen WG, Mohs RC, Davis KL. A new rating scale for Alzheimer's disease. Am. J. Psychiatry 1984;141(11):1356–1364
54. Farias ST, Mungas D, Reed BR, et al. The measurement of everyday cognition (ECog): scale development and psychometric properties. Neuropsychology 2008;22(4):531–44.
55. Pfeffer RI, Kurosaki TT, Harrah CH, et al. Measurement of functional activities in older adults in the community. [Internet]. J. Gerontol. 1982;37(3):323–9.